Int. J. Heat Mass Transfer. Vol. 34, No. 10, pp. 2461–2474, 1991
Printed in Great Britain

0017–9310/91 $3.00 + 0.00
© 1991 Pergamon Press plc

Three-dimensional modelling of the coupled flow field and heat transfer in continuous-flow electrophoresis

N. JOUVE and M. J. CLIFTON

Laboratoire de Génie Chimique et Electrochimie, U.R.A. CNRS 192, Université Paul Sabatier, 118 route de Narbonne, 31062 Toulouse Cedex, France

(*Received* 9 *July* 1990)

Abstract—A numerical model describing the steady, three-dimensional fluid flow and heat transfer in continuous-flow zone electrophoresis is developed to show the influence of gravitation on this process. It is capable of predicting undesirable effects, due to natural convection, such as back-flow and inlet and outlet disturbances. Comparison with a simpler two-dimensional model shows that the latter can be used to represent flow and heat transfer in the central part of the chamber. The simpler model is used to establish a correlation which gives the conditions beyond which back-flow occurs.

1. INTRODUCTION

A WIDE range of separation techniques has been developed for fractionating and purifying biological substances. Some of them are based on differences in biochemical properties, as in the case of affinity methods, others on differences in physico-chemical properties (size of the molecule, electrical charge). Although a few of these processes can be used to prepare small quantities of a product, of the order of 1 mg, they are generally used only for analytical purposes. In comparison with these techniques, the process of continuous-flow electrophoresis offers the advantage of allowing a continuous preparation or purification of biological products, with a production rate of about 1 mg h^{-1}, or even up to 1 g h^{-1}.

The operating principle is as follows (see Figs. 1 and 2). The sample containing the species to be separated (e.g. a mixture of proteins) is injected, through a capillary, into a liquid stream consisting of a buffer solution of known properties (pH, electrical conductivity, viscosity, etc.). This carrier buffer flows in the laminar regime between two flat, vertical plates forming a channel of constant thickness $2Z$, of length X and of width Y. Two electrode compartments, situated on either side of this chamber and separated from it by membranes, are used to apply a d.c. electric field across the width of the chamber. The membranes allow the electric current to pass while permitting the use of a fast-flowing electrode solution to remove the gases generated at the electrodes. The components of the injected sample are carried down the length of the chamber by the carrier flow, and migrate across the width of the chamber under the influence of the electric field, with a velocity which is proportional to the electric field strength and to the mobility of the species. This mobility depends on the electric charge of the molecule, on its size, on the viscosity of the surrounding medium, etc. The liquid stream containing the different species is collected at the outlet of the apparatus in a number of fractions, which correspond to the different mobilities.

Applying an electric field gives rise to various phenomena in the chamber. The passage of the electric current through the carrier buffer causes a diffuse generation of heat by the Joule effect. To prevent a rise in temperature of the solution along the length of the chamber, the walls are cooled by a fast-flowing liquid which can be considered as being at the constant temperature T_c^*. The temperature of the buffer circulating in the electrode compartments T_c^* can also be adjusted to reduce heating due to the resistance of the membranes. Furthermore, the passage of the electric current is made possible by the movement of the ions in the buffer. However, the transport numbers of these ions in the solution and in the membranes are different; as a result, concentration gradients appear

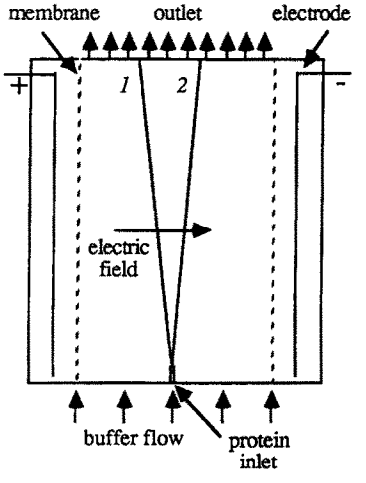

FIG. 1. Principle of continuous-flow electrophoresis: 1 and 2, two proteins with different mobilities.

NOMENCLATURE

A	dimensionless factor (equation (15a))
c	buffer concentration
C_p	heat capacity
e	thickness
E	electric field strength
g	gravity vector
h	heat transfer coefficient
k	thermal conductivity
P	dimensionless pressure
Q	dimensionless heat flux
r_m	area resistance of the membrane
R	electrical resistance
s	Joule heat source term
T	dimensionless temperature
T_0	inlet temperature of the buffer
U	potential difference applied to the electrodes
U_0	mean velocity
u, v, w	dimensionless velocity in the x-, y-, z-direction
V	velocity vector
x, y, z	dimensionless coordinates
X	length of the separation chamber
Y	width of the separation chamber
Z	half-thickness of the separation chamber.

Greek symbols

ε	dimensionless thickness of the polarization layer
μ	buffer viscosity
ρ	buffer density
σ	buffer electrical conductivity.

Subscripts

0	buffer, mean value
c	cooling compartment
e	electrode compartment
m	membrane
w	wall.

Superscript

*	dimensioned variable (for space, velocity, pressure and temperature).

Dimensionless numbers

Gr	Grashof number, $\rho_0 g \Delta\rho Z^3/\mu_0^2$
Pe	Peclet number, $\rho_0 C_p U_0 Z/k_0$
Re	Reynolds number, $\rho_0 U_0 Z/\mu_0$.

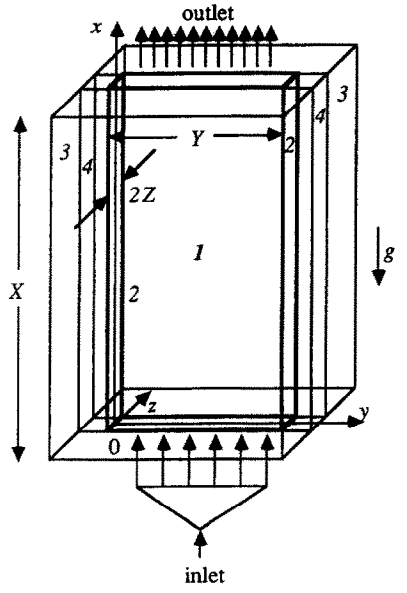

FIG. 2. Axes used in the numerical model: 1, separation chamber; 2, membrane; 3, cooled wall; 4, electrode compartment.

near the membrane surfaces. This is known as the membrane 'polarization' phenomenon; it leads on the one hand to a density profile having a direct influence on the flow, and on the other hand to an electrical conductivity profile, which implies a variation in the heat source term and a modification of the temperature profiles. In order to limit the effect of these phenomena, which can cause natural convection in addition to the desired forced convection of the carrier, and for reasons of hydrodynamic stability, the thickness $2Z$ of the chamber is in general very small compared with its other dimensions. The profile of the axial velocity u (in a y–z plane perpendicular to the flow) has a parabolic form in the z-direction. This means that the residence times of the species in the apparatus vary across the thickness of the chamber. Molecules having the same mobilities and situated at different values of z, will migrate at the same speed in the y-direction but for different times. Also, the walls of the chamber carry surface charges that are neutralized by ions in the solution. This mobile layer of ions, extremely thin compared with the chamber thickness, is set in motion by the electric field; this creates a slip velocity, the 'electro-osmotic' velocity, on the walls of the cell in the direction of the field. As the sides of the chamber are closed off by the watertight membranes, there is a return flow of liquid along the central x–y plane of the cell. In this way, a lateral velocity, in the y–z plane, is set up also having a parabolic profile in the z-direction. These two phenomena, the distribution of residence times and the electro-osmotic flow, cause a deformation of the

injected sample stream: its cross-section, initially circular at the inlet, takes on a crescent form.

Several simplified mathematical models for the flow and heat transfer have been developed in recent years. The simple one-dimensional model only takes into account the variations in velocity and temperature across the chamber thickness. The Navier–Stokes equation and the heat transfer equation can then be integrated analytically to give the velocity and temperature profiles, e.g. to find the cooling temperature to be used. The temperature profile obtained only has an effect on the flow under the most extreme operating conditions, i.e. at high field strengths, in thick chambers, conditions well beyond those for which the membrane polarization begins to become important. Several two-dimensional models have also been developed in which velocity variations in the x-direction are neglected [1–3]. They take into account the electro-osmotic flow and the coupling between the heat transfer and the axial flow. The polarization phenomenon and the flow variations at the inlet and outlet of the cell are neglected.

Experimental observations performed in our laboratory have shown that under certain conditions the stream of injected sample deviates from its initial straight trajectory; this can only be explained by variations of the flow field in the x-direction. It shows the importance of natural convection, particularly that due to the polarization layers. By upsetting the flow in the cell, it compromises the quality of the separation.

The use of this process in microgravity has been envisaged. It would thus be freed of the natural convection effects which limit its operating conditions on earth. Such a treatment might indeed be worth considering in the case of some very expensive biological products. However, even in such circumstances, if one is to justify operation in microgravity, a clear knowledge of its advantages is required. The aim of the present work is to show the principal effects of gravity on this process and so more clearly define the limits imposed on it by earth-based operation.

A computer code in which the three-dimensional and coupled Navier–Stokes and heat transfer equations are solved has been developed. Combined with a code for calculating the transfer of the sample substances under the influence of the flow field, electrophoretic migration and molecular diffusion, it is possible to compare its predictions with experimental observations of protein separation. Furthermore, a study of the calculated velocity fields makes it possible to define the limiting operating conditions which can be used on earth. In a microgravity environment, the limits are quite different and are essentially related to the capacity of the cooling system and to the overall energy consumption of the device. This code can also be used for designing the apparatus so as to find the optimum size of the cell to suit the aim which has been fixed, i.e. the desired compromise between production rate and purity.

2. MATHEMATICAL MODEL

2.1. *Navier–Stokes and heat transfer equations*

As the equipment is intended for continuous production, the equations will be used in their steady-state form. The system of axes is defined in Fig. 2. We shall make the following assumptions:

(i) the carrier buffer is a Newtonian fluid,

(ii) the temperature differences are small, so the viscosity and the various thermal conductivities can be considered as constant,

(iii) non-uniformities in density, due to variations in temperature and concentration are only taken into account in the source term of the momentum equation,

(iv) the variations in electrical conductivity, however, are entirely taken into account,

(v) the viscous dissipation of heat is neglected,

(vi) the lines of electrical current are parallel to the y-axis.

After adopting the following dimensionless variables:

$$\begin{bmatrix} x \\ y \\ z \end{bmatrix} = \begin{bmatrix} x^*/Z \\ y^*/Z \\ z^*/Z \end{bmatrix} \tag{1a}$$

$$V = \frac{V^*}{U_0} \tag{1b}$$

$$P = \frac{P^* - \rho_0 g x^*}{\rho_0 U_0^2} \tag{1c}$$

$$T = \frac{k_0}{Z^2} \frac{T^* - T_0}{\sigma_0 E_0^2} \tag{1d}$$

and writing the Reynolds, Peclet and Grashof numbers in the following forms:

$$Re = \frac{Z U_0 \rho_0}{\mu_0} \tag{2a}$$

$$Pe = \frac{Z C_{p_0} \rho_0 U_0}{k_0} \tag{2b}$$

$$Gr = \frac{\Delta\rho}{\rho_0} \frac{Z^3 \rho_0^2 g}{\mu_0^2} \tag{2c}$$

the Navier–Stokes and heat transfer equations can be written in the steady state as follows:

$$\text{div}\,(V) = 0 \tag{3}$$

$$V \cdot \text{grad}\, V = -\text{grad}\, P + \frac{1}{Re} \text{div grad}\, V + \frac{Gr}{Re^2} \tag{4}$$

$$V \cdot \text{grad}\, T = \frac{1}{Pe} \text{div grad}\, T + \frac{s}{Pe\, \sigma_0 E_0^2}. \tag{5}$$

2.2. *Boundary conditions for the velocity*

(a) At the entrance to the cell ($x = 0$), the velocity component u is given as a fully developed laminar

flow, i.e.

$$\frac{\partial u}{\partial x} = 0$$

$v = 0$ and $w = 0$ and the density is uniform.

The momentum equations are then reduced to the following:

$$\frac{1}{Re}\left[\frac{\partial^2 u}{\partial y^2} + \frac{\partial^2 u}{\partial z^2}\right] = \frac{\partial P}{\partial x} \tag{6}$$

and

$$\frac{\partial P}{\partial y} = \frac{\partial P}{\partial z} = 0.$$

Thus P is a function of x only and the left-hand side of the first equation is only a function of y and z. In this equation, therefore, a function of y and z is set equal to a function of x; as these are independent variables, each of the two terms is equal to a constant and we obtain

$$\frac{\partial^2 u}{\partial y^2} + \frac{\partial^2 u}{\partial z^2} = C. \tag{7}$$

The other velocity components are zero

$$v = w = 0.$$

(b) At the outlet of the cell ($x = X/Z$), the liquid is drawn off at the same rate by all the tubes of the fraction collector. This is represented by

$$u = \text{constant, and } v = w = 0.$$

(c) The membranes at $y = 0$ and Y/Z are impermeable to water; this leads to

$$u = v = w = 0.$$

(d) On the walls of the cell ($z = 1$), only the v component is non-zero. It is equal to the electro-osmotic slip velocity, i.e.

$$u = w = 0$$

$$v = v_{os}.$$

(e) On the central plane of the cell ($z = 0$), the symmetry condition implies that

$$\left(\frac{\partial u}{\partial z}\right)_{z=0} = \left(\frac{\partial v}{\partial z}\right)_{z=0} = \left(\frac{\partial w}{\partial z}\right)_{z=0} = 0.$$

2.3. *Boundary conditions for the temperature*

The limiting conditions for the temperature are rather more complex, as they represent the cooling via the walls and via the membranes, as well as the Joule heating within the membranes.

(a) At the inlet to the cell (at $x = 0$), the temperature is uniformly equal to T_0, thus

$$T = 0.$$

(b) The walls of the cell (at $z = 1$), of thickness e_w and thermal conductivity k_w, are cooled on their outer faces by a liquid at the constant temperature T_c (Fig. 3). If h_w is the heat-transfer coefficient at the interface between the wall and the cooling compartment, then the equality of the dimensionless heat fluxes at the two interfaces of the wall may be written as

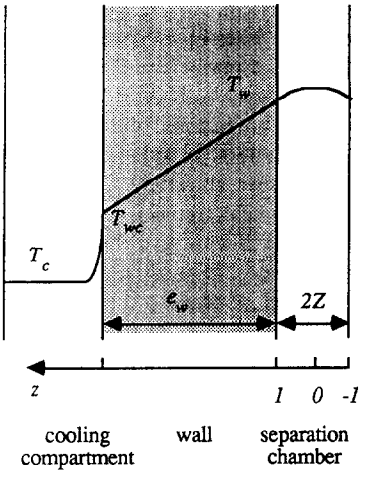

FIG. 3. Boundary condition for temperature at the wall.

$$Q_w = \frac{1}{Pe}\frac{k_w Z}{k_0 e_w}(T_w - T_{wc})$$

$$= \frac{1}{Pe}\frac{Z h_w}{k_0}(T_{wc} - T_c) = \frac{1}{Pe}\left(\frac{\partial T}{\partial z}\right)_w.$$

Eliminating T_{wc} from these expressions, we obtain the desired relationship

$$\frac{1}{Pe}\left(\frac{\partial T}{\partial z}\right)_w = -\frac{1}{Pe}\frac{Z h_w k_w}{k_0(h_w e_w + k_w)}(T_w - T_c). \tag{8}$$

(c) The membranes (at $y = 0$ and Y/Z), of thickness e_m and thermal conductivity k_m, are subjected to heat generation from a Joule source s_m (Fig. 4). The solu-

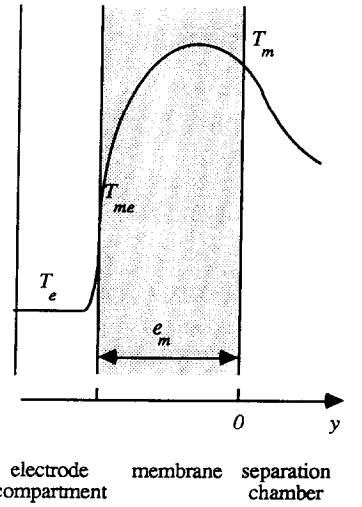

FIG. 4. Boundary condition for temperature at the membrane.

tion circulating in the electrode compartments is at a constant temperature T_e^*, and the heat-transfer coefficient at the membrane surface in the electrode compartment is h_m. The heat-transfer equation for the membrane may be written as

$$\frac{1}{Pe}\frac{k_m}{k_0}\frac{\partial^2 T}{\partial y^2}+\frac{s_m}{Pe\,\sigma_0 E_0^2}=0.$$

The boundary conditions for this equation represent the conservation of heat flux at the membrane–carrier solution interface

$$Q_m=\frac{1}{Pe}\frac{k_m}{k_0}\left(\frac{\partial T}{\partial y}\right)_{me}=\frac{1}{Pe}\frac{Zh_m}{k_0}(T_{me}-T_e)$$

and at the membrane–electrode solution interface

$$Q'_m=\frac{1}{Pe}\frac{k_m}{k_0}\left(\frac{\partial T}{\partial y}\right)_{m-}=\frac{1}{Pe}\left(\frac{\partial T}{\partial y}\right)_{m+}.$$

Integrating the heat-transfer equation for the membrane and eliminating the temperature T_{me}, we obtain the expression for the heat flux at the membrane–carrier buffer interface

$$\frac{1}{Pe}\left(\frac{\partial T}{\partial y}\right)_m=\frac{1}{Pe}\left[\frac{Zh_m k_m}{k_0(Zh_m e_m+k_m)}(T_m-T_c)-\frac{s_m e_m}{\sigma_0 E_0^2(Zh_m e_m+k_m)}\left[\frac{Zh_m e_m}{2}+k_m\right]\right]. \quad (9)$$

(d) In the central plane (at $z=0$), symmetry implies that

$$\left(\frac{\partial T}{\partial z}\right)_{z=0}=0.$$

2.4. *Joule heat source term*

The source term in the heat-transfer equation takes into account the heat generated in the bulk solution by the Joule effect. We shall make the following assumptions:

(i) the lines of electric current are parallel to the y-axis,

(ii) U is the potential difference applied to the electrodes,

(iii) the electrical resistance of the electrode compartments can be neglected,

(iv) r_m is the area resistance of the membranes ($\Omega\,m^2$),

(v) σ_{xyz}, the electrical conductivity at the point (x, y, z), is a function of the temperature and of the ion concentration at this point.

The current varies with x and z. The current density can be expressed in the form

$$i_{xz}=\frac{1}{\Delta x\Delta z}\frac{U}{R_{xz}}$$

where R_{xz} is the electrical resistance of a volume element of cross-section $\Delta x\Delta z$, extending from one membrane to the other

$$R_{xz}=\int_{-e_m}^{Y+e_m} r_{xyz}\,dy=2\frac{r_m}{\Delta x\Delta z}+\frac{1}{\Delta x\Delta z}\int_0^Y\frac{dy}{\sigma_{xyz}}.$$

For the current passing through the volume element $\Delta x\Delta y\Delta z$ the following expression is found:

$$I_{xz}=\Delta x\Delta z\frac{U}{2r_m+\int_0^Y\frac{dy}{\sigma_{xyz}}}.$$

The rate of energy dissipation per unit volume of solution can then be written as

$$s=\left[\frac{U}{2r_m+\int_0^Y\frac{dy}{\sigma_{xyz}}}\right]^2\frac{1}{\sigma_{xyz}}. \quad (10)$$

In the same way the expression for the heat source in the membrane is obtained as

$$s_m=\left[\frac{U}{2r_m+\int_0^Y\frac{dy}{s_{xyz}}}\right]^2\frac{r_m}{e_m}. \quad (11)$$

2.5. *Numerical solution*

The numerical integration of the system of differential equations was performed by a finite-difference method, derived from the SIMPLE algorithm (semi-implicit method for pressure-linked equations) developed by Patankar [4]. The grid used is of the MAC (marker-and-cell) type, in which the points where the three velocity components, u, v and w, are defined are displaced by a half step from the points where the other variables (pressure, temperature, density, conductivity) are defined. The equations are discretized on this grid following the hybrid scheme proposed by Patankar; in this scheme, diffusion–convection terms are discretized using a combination of upwind and centred differences dependent on the local velocity values. This avoids numerical diffusion problems which can arise for certain values of the Reynolds and Grashof numbers.

The discretization of the x-direction momentum equation leads to an equation of the following type for each point p of the grid (Fig. 5):

$$a_p u_p=a_n u_n+a_s u_s+a_e u_e+a_w u_w+a_t u_t+a_b u_b+\frac{P_P-P_E}{\Delta x}+\frac{Gr_P}{Re^2}. \quad (12)$$

An equation of the same type is obtained for the components v and w, as well as for the temperature.

The principle of the solution method consists in starting from an estimated pressure distribution P^*. The momentum and heat equations, equations (4) and (5), are solved on the basis of P^*, which gives V^*

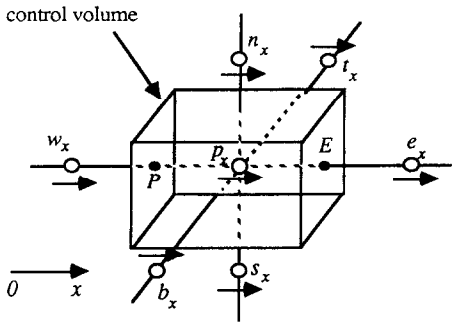

FIG. 5. Discretization cell for the x-direction momentum equation.

and T^*. The divergence of the velocity field V^* is non-zero. One then considers the velocity corrections V' and the pressure corrections P' such that the velocity field $V = V^* + V'$, corresponding to the pressure distribution $P = P^* + P'$, satisfies the continuity equation (3). By subtracting the momentum equation for V and P from the momentum equation for V^* and P^*, the following relating V' and P' is obtained, in the form for the x component:

$$u'_{P_x} = \sum_{1}^{6} \frac{a_{nb}}{a_{P_x}} u'_{nb} + \frac{P'_P - P'_E}{a_{P_x} \Delta x}. \quad (13)$$

At this point, Patankar recommends neglecting the velocity corrections at the neighbouring points; this means that, once the pressure corrections have been calculated, the field V' can be obtained explicitly and used to correct the velocities by putting $V = V^* + V'$. In our case, because of the peculiar geometry of the cell (aspect ratio of the type $Z \ll Y \ll X$) and because of the very low Reynolds numbers (1–5), it was found to be necessary not to neglect these terms if convergence was to be achieved. A pressure-correction equation can be obtained by considering the discretization coefficients as constant. By taking the divergence of the equation relating P' to V' and by writing

$$\text{div}\,(V) = \text{div}\,(V^*) + \text{div}\,(V') = 0$$

we obtain an equation, written for point P, relating the pressure corrections to the value of the divergence of V^*

$$a_P P'_P = a_N P'_N + a_S P'_S + a_E P'_E + a_W P'_W + a_T P'_T + a_B P'_B - \text{div}\,(V^*)_P + \sum_{1}^{6} \frac{a_{nb}}{a_P} \text{div}\,(V^*)_{nb}. \quad (14)$$

The solution of the system represented by this equation, written for each point of the grid, leads to a field of pressure corrections P'. The pressure distribution $P = P^* + P'$ constitutes a new estimate P^*, leading to a new field V^* closer to the continuity requirement. In this way an iterative procedure has been set up which can be summarized by the algorithm in Fig. 6.

It should be noted that the approximation introduced to arrive at equation (14) has no influence on the final solution. Once the field V^* satisfies the continuity condition, equation (14) allows the particular solution $P' = 0$ at each point on the grid.

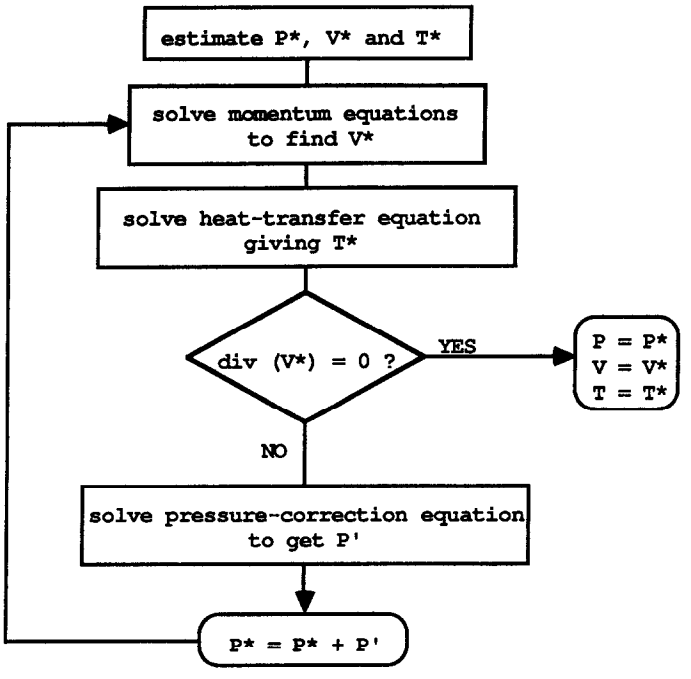

FIG. 6. Algorithm used in the numerical model.

3. RESULTS

3.1. *Influence of heat transfer alone*

In order to prevent Joule heating from raising the temperature of the carrier buffer as it flows through the cell, the walls of the cell, as was previously explained, are cooled by a liquid of constant temperature T_c^*. We shall now consider that T_c^* is chosen such that the overall temperature difference in the x-direction, from the inlet to the outlet, is zero. Instabilities due to density gradients in the flow direction will not be considered [5].

The cooling via the walls gives rise to a temperature gradient in the z-direction. The effects due to this gradient, previously studied using one-dimensional [6] and two-dimensional models [1–3] are confirmed by the three-dimensional model. It disturbs the almost parabolic profile in the z-direction in the following way:

$$u(z) = \tfrac{3}{2}(1-z^2)\left[\frac{A}{18}\left(z^2-\frac{1}{5}\right)+1\right] \qquad (15a)$$

with

$$A = \frac{\rho_0 g \beta \sigma_0 E_0^2 Z^4}{2\mu_0 k_0 U_0}. \qquad (15b)$$

Alterations in the performance of the process due to this phenomenon (changes in the way the crescent deformation varies with mobility) begin to appear only for intense electric fields in thick chambers (about 5000 V m^{-1} in 3 mm thick chambers). Instabilities arise only at even higher field strengths (about 20 000 V m^{-1}), causing back-flows in the centre for downward flows, near the walls for upward flows. With the membranes and the buffers used at present, the disturbances induced by the polarization layers develop under much milder conditions, so we shall now concentrate on them.

3.2. *Influence of the polarization layers*

The development of the polarization layers near the membranes is a complex phenomenon depending on the buffer and membrane properties, on the electrical current, on the flow rate, etc. Providing a correct representation of this phenomenon is a considerable task and is beyond the scope of the present work. It is known that these layers grow rapidly in thickness near the inlet of the channel, then grow much more slowly. We shall assume for the sake of simplicity that the concentration profiles are invariant with x and with z and have a given form and thickness in the y-direction

$$c = f(y). \qquad (16)$$

Measurements made at the outlet of the chamber have led us to consider the following function for the buffer concentration:

$$c(y) = c_0 + (c_m - c_0)\left(1 - \sin\frac{\pi y}{2\varepsilon}\right) \quad \text{for } 0 < y < \varepsilon \qquad (17a)$$

$$c(y) = c_0 \quad \text{for } \varepsilon < y < \frac{Y}{Z} - \varepsilon \qquad (17b)$$

$$c(y) = c_0 + (c_m - c_0)\left(1 - \sin\frac{\pi(Y/Z-1)}{2\varepsilon}\right) \quad \text{for } \frac{Y}{Z} - \varepsilon < y < \frac{Y}{Z}. \qquad (17c)$$

Here ε is the thickness of the polarization layers, dimensionless in relation to Z. Empirical correlations are used to represent the variations in density and electrical conductivity of the tris-borate buffer with concentration and temperature.

The polarization layers thus have a twofold influence on the flow pattern: firstly a direct effect due to concentration-related density differences, secondly an indirect effect due to variations in conductivity, causing temperature differences, which in turn produce additional density variations. We begin by considering the first, direct influence. An example of a calculated flow map is shown in Figs. 7 and 8; this corresponds to the case where both membranes are of the same polarity (e.g. both cation-exchange). This means that the buffer solution becomes more concentrated on one side of the chamber and is depleted in ions on the other. The disturbances in the flow profile near the membranes produce compensating flows at the inlet and outlet of the chamber, and thus cause the sample stream to deviate (Fig. 9).

3.3. *Flow stability with polarization*

Flow maps have been calculated without taking into account the coupling with heat transfer; they are for a chamber 60 cm long, 6 cm wide and of variable thickness $2Z$, for different values of c_m and of the mean velocity U_0. Profiles of the u velocity component in the central y–z plane at $x = 30$ cm are shown in Figs. 10–13. Examining the overall velocity field (Fig. 7), it can be seen that these profiles, for reasonable electric fields (< 10 000 V m^{-1}), are independent of the inlet and outlet effects, particularly the compensating movements, as well as the electro-osmotic motion. It can then be considered that these central velocity profiles can be calculated using a two-dimensional equation in which the gradients in the x-direction are neglected as well as the advection terms [1]

$$\frac{1}{Re}\left(\frac{\partial^2 u}{\partial y^2} + \frac{\partial^2 u}{\partial z^2}\right) = \frac{\partial P}{\partial x} - \frac{Gr(y)}{Re^2}. \qquad (18)$$

For the same reasons as those invoked in the discussion of the inlet flow field (Section 2.2(a)), we arrive at the following relationship, cf. equation (7):

$$\frac{\partial^2 u}{\partial y^2} + \frac{\partial^2 u}{\partial z^2} = C - \frac{Gr(y)}{Re}. \qquad (19)$$

The dimensionless velocity profile obtained by solving this equation thus depends on the local values of

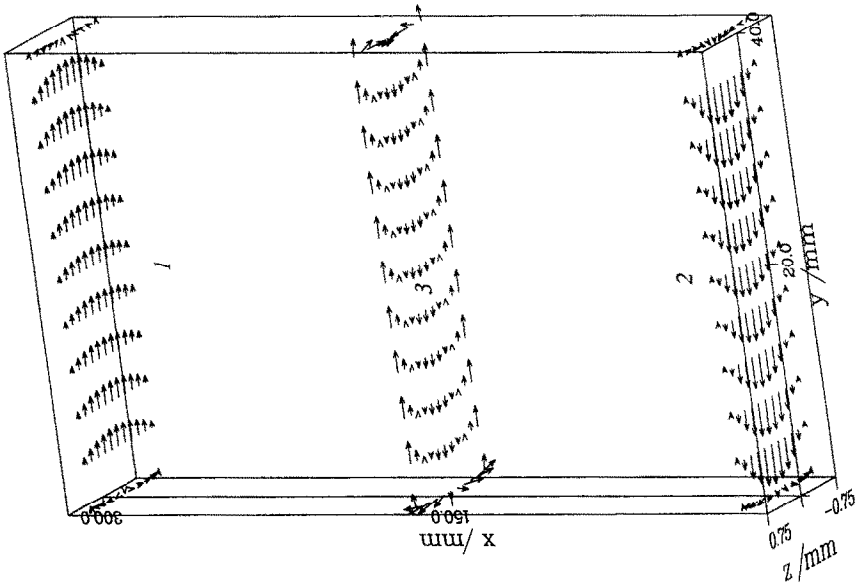

FIG. 8. Transverse velocity distribution : 1 and 2, compensating flows ; 3, electro-osmotic flow.

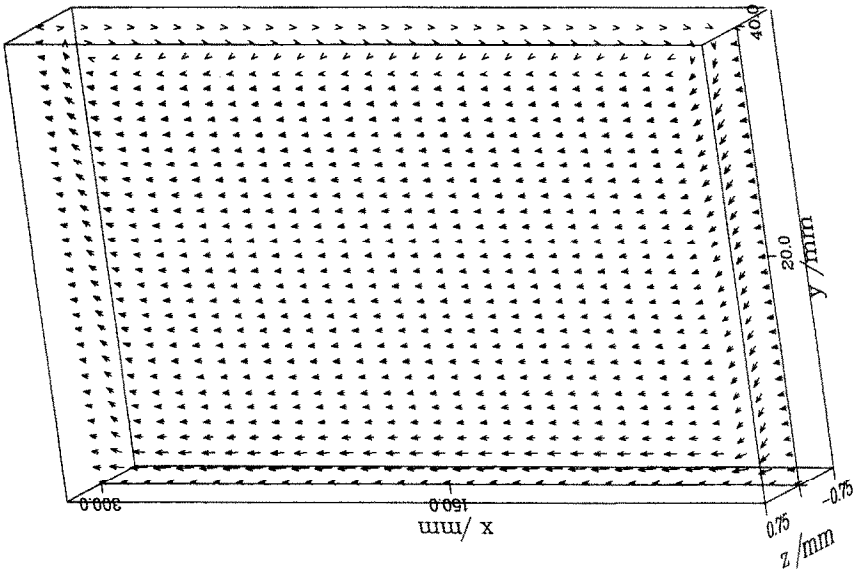

FIG. 7. Velocity distribution in the central plane of the cell ($z = 0$).

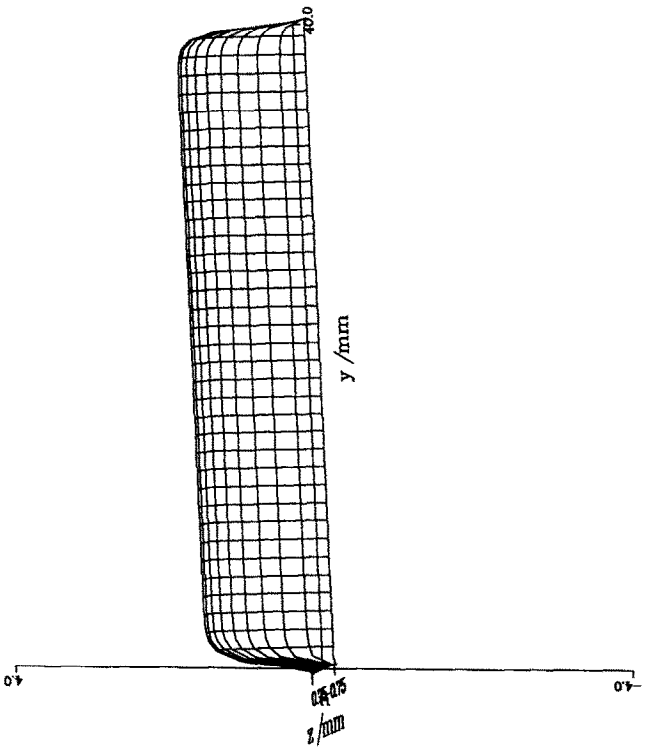

FIG. 10. Poiseuille profile for u at the mid-length of the cell ($x = X/2Z$).

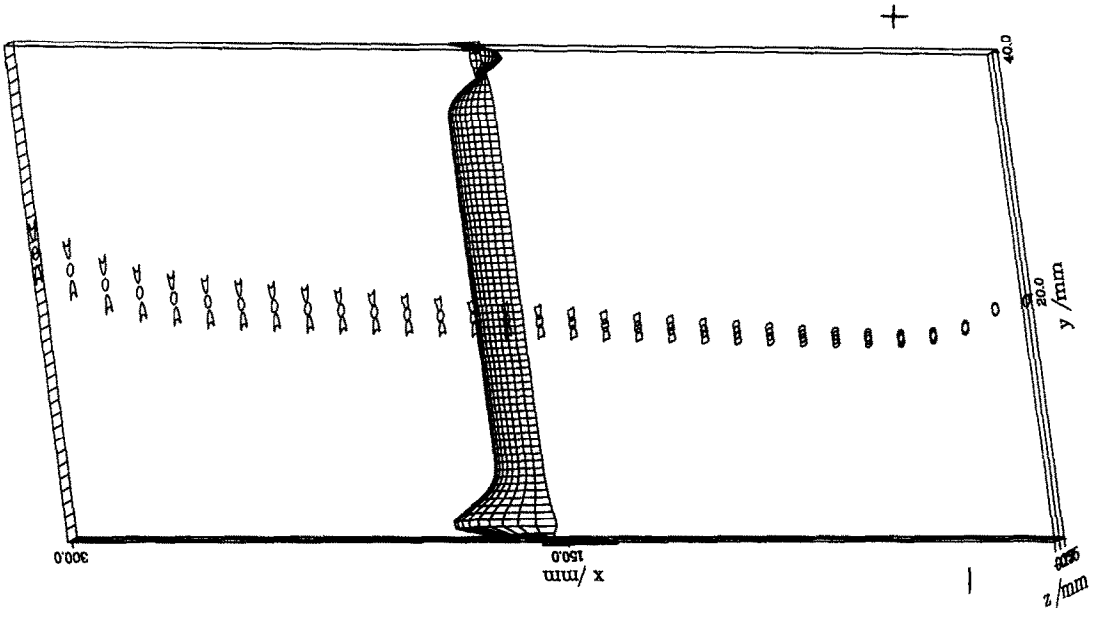

FIG. 9. Deviation of the protein stream when natural convection occurs: three proteins with different mobilities.

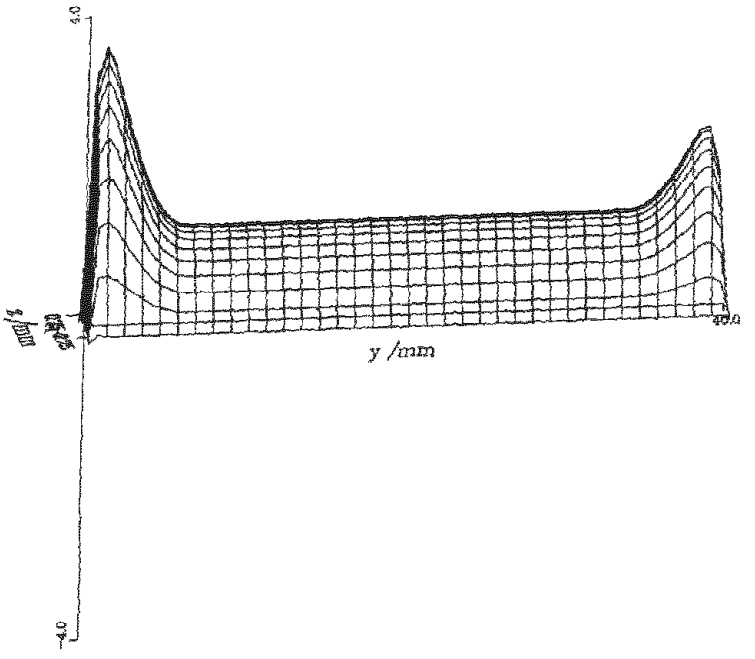

FIG. 11. Velocity profile for u at the mid-length of the cell for two membranes of different polarities, downflow.

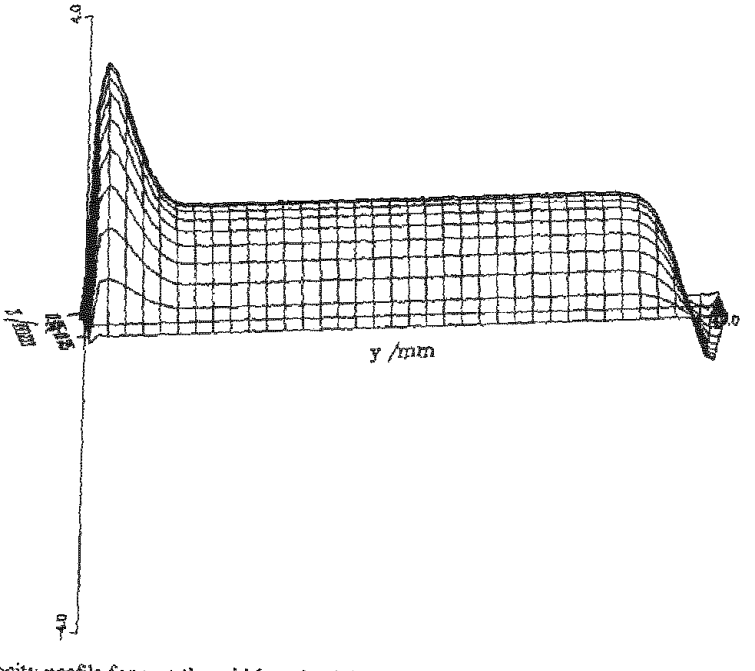

FIG. 12. Velocity profile for u at the mid-length of the cell for two membranes with the same polarity.

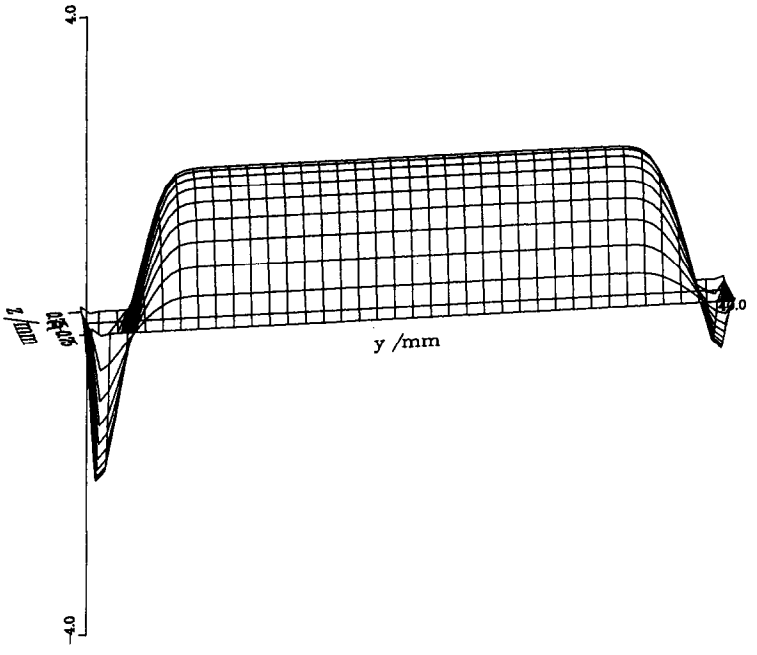

FIG. 13. Velocity profile for u at the mid-length of the cell for two membranes of different polarities, upflow.

Gr/Re, and so on $\Delta\rho_m$, ε and the function f, as well as on the aspect ratio Y/Z. Moreover, it can be expressed as the sum of the profiles which are solutions of the two following partial differential equations:

(i) the equation giving the forced-convection profile, a function of Y/Z only

$$\frac{\partial^2 u_1}{\partial y^2} + \frac{\partial^2 u_1}{\partial z^2} = C; \tag{20}$$

(ii) the natural-convection equation, whose solution depends on Gr_m/Re, ε, on the function f, as well as on Y/Z

$$\frac{\partial^2 u_2}{\partial y^2} + \frac{\partial^2 u_2}{\partial z^2} = -\frac{Gr(y)}{Re}. \tag{21}$$

It is important to define conditions which will give rise to a back-flow, as this can lead to the formation of re-mixing zones which would impair the separation process. The limiting condition for the appearance of a back-flow is

$$\left(\frac{\partial u}{\partial y}\right)_{y=0} = 0.$$

Now this gradient can be written in the form

$$\left(\frac{\partial u}{\partial y}\right)_{y=0} = h_1\left(\frac{Y}{Z}\right) + h_2\left(\frac{Y}{Z}, \frac{Gr_m}{Re}, \varepsilon, f\right). \tag{22}$$

The function h_1 arises from the solution to equation (20), while the function h_2 comes from the solution to equation (21). The condition for a zero gradient at the membrane then becomes

$$\frac{Gr_m}{Re} = h_3\left(\frac{Y}{Z}, \varepsilon, f\right). \tag{23}$$

The function h_3 has been evaluated, using the function f defined by equations (17), for different values of Y/Z and ε. Small variations of h_3 with the aspect ratio Y/Z are observed. The values of Gr_m/Re giving a zero gradient have been plotted as a function of ε, for two extreme values of Y/Z (Fig. 14). The insets in this figure show the types of velocity profile which appear near the membranes for different values of Gr_m/Re.

From this curve, given the dimensions of the chamber (width, thickness) and the operating conditions (mean flow velocity, buffer viscosity, etc.), the values of $\Delta\rho_m$ and ε can be determined beyond which a back-flow will occur. The values of $\Delta\rho_m$ and ε can be related to a value of the electric field, after a series of measurements with the buffer, the pH and the membranes previously chosen.

3.4. *The influence of polarization layers on heat transfer*

We have seen that the polarization layers lead to a conductivity profile in the y-direction. This causes

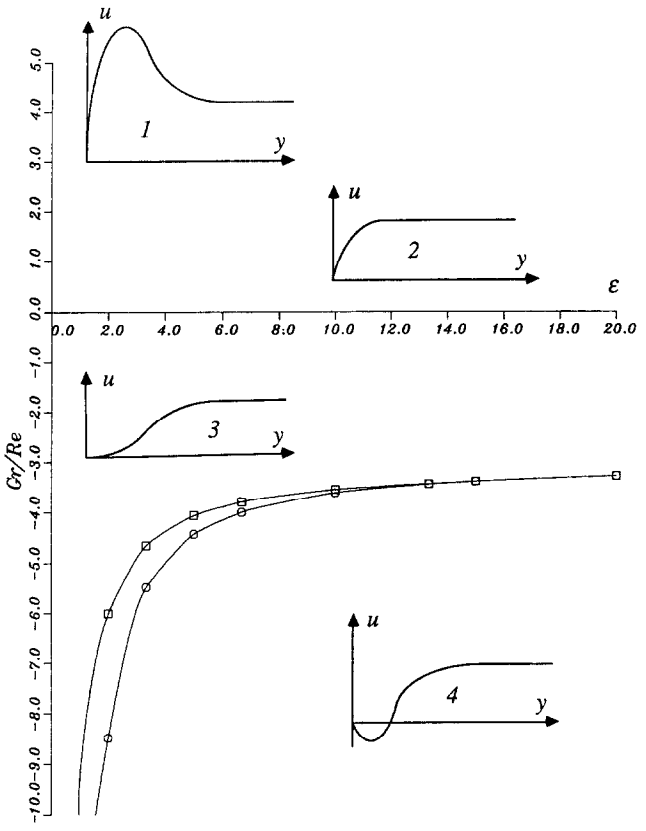

FIG. 14. As a function of ε, the value of Gr/Re at the membrane leading to a zero-gradient for u in the y-direction: 1, increasing velocity in the polarization layer; 2, Poiseuille flow; 3, limiting condition before back-flow occurs; 4, polarization layer leading to back-flow (□, $Y/Z = 26.7$; ○, $Y/Z = 107$).

non-uniformities in the Joule heat source term in the zones near the membranes. Several cases can be envisaged depending on the buffer and the membranes used. With two cation-exchange membranes, the variations in electrical conductivity lead to a temperature profile such as that shown in Fig. 15.

Generally speaking, if the buffer used is a low conductivity one, such as is used normally in electrophoresis, and if the temperature gradient in the flow direction is small, then the variations in concentration of the buffer species have a greater effect on the density by their direct influence than by their effect on the temperature via the conductivity. The two types of influence can, in some rare situations, act in opposite directions but in most cases a drop in buffer concentration lowers both the density and the conductivity (thus causing greater heating), so the two effects act in the same sense. There is, in all cases, a certain heating up of the solution near the chamber sides due to the resistance of the two membranes. The influence of these heat-transfer effects can only be obtained by a complete three-dimensional solution of the system of equations, such as our code is capable of producing. This calculation makes it possible, in particular, to adjust the temperatures of the cooling liquid but also of the electrode solutions so as to minimize natural convection, especially that due to the presence of polarization layers.

4. CONCLUSION

From the experience acquired with a full three-dimensional model for the flow and heat transfer in a continuous-flow electrophoresis chamber, there are several conclusions which can be drawn. On the one hand it was found that the complete model is capable of predicting behaviour, such as the non-linear sample trajectories, observed experimentally but not predictable by the earlier, simpler models. On the other hand, it was also confirmed that a two-dimensional model could be used as a good guide to the flow behaviour over the major part of the chamber length. The two-dimensional version of the model was used to find a correlation which can be used to predict conditions under which back-flow is avoided. To apply this correlation with precision, an experimental study of the membrane polarization effects would be necessary, but from the information already available, it is clear that the microgravity environment can offer real advantages in improving the resolution of electrophoresis separations. The chambers at present used on earth are in fact operating quite close to the limits

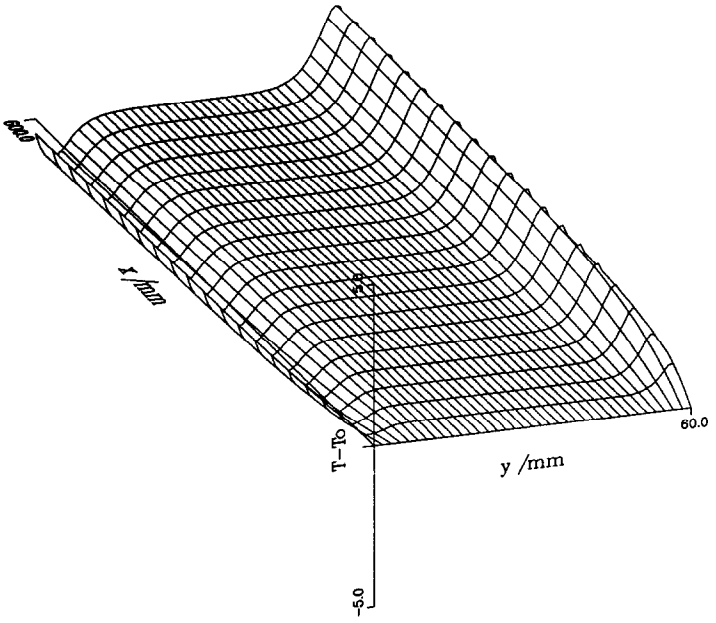

FIG. 15. Temperature distribution in the $z = 0$ plane in a cell with two cation-exchange membranes.

imposed by requirements of flow stability and reproducibility. Other studies [7] have shown that improvements in resolution can be obtained, for example, by using thicker chambers, but under the conditions of the earth's gravity, the flow regime would no longer be satisfactory.

Acknowledgement—This work was undertaken with the financial support of the French space agency, the Centre National d'Etudes Spatiales (CNES).

REFERENCES

1. J. A. Deiber and D. A. Saville, Flow structure in continuous-flow electrophoresis chambers. In *Materials Processing in the Reduced Gravity Environment of Space* (Edited by G. E. Rindone). Elsevier, Amsterdam (1982).
2. P. H. Rhodes and R. S. Snyder, Numerical analysis of continuous flow electrophoresis. In *Electrophoresis '81* (Edited by R. C. Allen and P. Arnaud). Walter de Gruyter, Berlin (1981).
3. M. J. Clifton and O. Marsal, Heat-transfer design of an electrophoresis experiment, *Acta Astronautica* **19**, 99–103 (1989).
4. S. V. Patankar, *Numerical Heat Transfer and Fluid Flow*. Hemisphere, New York (1980).
5. S. Ostrach, Convection in continuous flow electrophoresis, *J. Chromatog.* **140**, 187–195 (1977).
6. F. Escale, Etude du fonctionnement d'une cellule d'électrophèse de zone à écoulement continu au sol en vue d'expérimentations en microgravité, Thèse Dr. Ing., Université Paul Sabatier, Toulouse, France (1987).
7. M. J. Clifton, N. Jouve, H. de Balmann and V. Sanchez, Conditions for purification of proteins by free-flow zone electrophoresis, *Electrophoresis* **11**, 913–919 (1990).

MODELISATION TRIDIMENSIONNELLE DES ECOULEMENTS ET DU TRANSFERT THERMIQUE COUPLES EN ELECTROPHORESE A ECOULEMENT CONTINU

Résumé—Un modèle numérique qui décrit, en trois dimensions et à l'état stationnaire, l'hydrodynamique et le transfert thermique dans l'électrophorèse de zone à écoulement continu a été développé en vue de montrer l'influence de la gravité sur ce procédé. Le modèle rend compte d'effets néfastes, dus à la convection naturelle, tels que les courants de retour et les perturbations d'entrée et de sortie. La comparaison avec un modèle bi-dimensionnel plus simple montre que ce dernier peut servir pour représenter l'écoulement et le transfert de chaleur dans la partie centrale de la chambre. Le modèle bi-dimensionnel a permis d'établir une corrélation qui prévoit les conditions au delà desquelles se forment des courants de retour.

DREIDIMENSIONALE MODELLIERUNG VON STRÖMUNGSFELD UND WÄRMEÜBERGANG BEI DER ELEKTROPHORESE IN KONTINUIERLICHER STRÖMUNG

Zusammenfassung—Ein numerisches Modell zur Beschreibung der stationären dreidimensionalen Strömung und des Wärmeübergangs in einer kontinuierlich durchströmten Elektrophorese wird entwickelt, um den Einfluß der Schwerkraft auf diesen Vorgang zu zeigen. Das Modell ist in der Lage, unerwünschte Einflüsse aufgrund der natürlichen Konvektion (wie Rückströmung und Störungen durch Ein- und Auslaß) vorauszuberechnen. Der Vergleich mit einem einfacheren zweidimensionalen Modell zeigt, daß dieses dazu geeignet ist, Strömung und Wärmeübergang im Zentrum der Kammer darzustellen. Das einfachere Modell wird verwendet, um eine Beziehung für Betriebsbedingungen aufzustellen, bei denen keine Rückströmung auftritt.

ТРЕХМЕРНОЕ МОДЕЛИРОВАНИЕ ВЗАИМОСВЯЗАННЫХ ПОЛЯ ТЕЧЕНИЯ И ТЕПЛОПЕРЕНОСА ПРИ ЭЛЕКТРОФОРЕЗЕ В ПОТОКЕ

Аннотация—Разработана численная модель, описывающая стационарное трехмерное течение жидкости и теплоперенос при электрофорезе с целью определения влияния гравитации на исследуемый процесс. Модель позволяет предсказывать такие нежелательные эффекты, вызванные естественной конвекцией, как, например, обратные течения, а также возмущения на входе и выходе. Сравнение с более простой двумерной моделью показывает, что последняя может использоваться для описания течения и теплопереноса в центральной части камеры. Упрощенная модель применяется для получения обобщенного выражения, определяющего условия возникновения противотока.